CARBON 88 (2015) 165–172

Available at www.sciencedirect.com

ScienceDirect

journal homepage: www.elsevier.com/locate/carbon

Hybrid structures of organic dye and graphene for ultrahigh gain photodetectors

Youngbin Lee [a,1], Seong Hun Yu [b,1], Jiwon Jeon [d], Hyunmin Kim [e], Jun Young Lee [b], Hyungjun Kim [d], Jong-Hyun Ahn [f,*], Euyheon Hwang [a,c,*], Jeong Ho Cho [a,b,*]

[a] SKKU Advanced Institute of Nanotechnology (SAINT), Sungkyunkwan University, Suwon 440-746, Republic of Korea
[b] School of Chemical Engineering, Sungkyunkwan University, Suwon 440-746, Republic of Korea
[c] Department of Physics, Sungkyunkwan University, Suwon 440-746, Republic of Korea
[d] Graduate School of Energy, Environment, Water, and Sustainability (EEWS), Korea Advanced Institute of Science and Technology, Daejeon 305-701, Republic of Korea
[e] Nano & Bio Research Division, Daegu Gyeongbuk Institute of Science and Technology, Daegu 711-873, Republic of Korea
[f] School of Electrical and Electronic Engineering, Yonsei University, Seoul 120-749, Republic of Korea

ARTICLE INFO

Article history:
Received 20 December 2014
Accepted 26 February 2015
Available online 5 March 2015

ABSTRACT

A hybrid structure comprising organic dye molecules (e.g., rhodamine 6G) and graphene was developed for the realization of high-performance optoelectronic devices. The fabricated photodetector offered a broad spectral photo-response across wavelengths in the infrared, visible, and ultraviolet regions, as well as a high responsivity (~460 A/W at illumination power of 1 μW). The photocurrent generated in the hybrid photodetector (~mA) was much higher than that generated in a pristine graphene photodetector (<μA). The performance of the dye-sensitized photodetector relied on enhanced photoabsorption and the implementation of a photocurrent gain arising from the photo-excited charges.

1. Introduction

Graphene enables new approaches toward the realization of high performance photonic and optoelectronic devices [1,2]. Graphene-based photodetectors have received considerable attention because their spectral bandwidths are broad compared to those of semiconductor-based photodetectors [3–6]. The optical absorption coefficient of graphene is almost constant from the visible to the infrared wavelengths because of the band structure of graphene [7] (i.e., a zero band gap and a linear energy dispersion); however, the weak light absorption of the atomically thin graphene layer and the very low gain mechanisms (e.g., carrier multiplication) have limited key properties that are needed for high-performance photodetectors, including the quantum efficiency, responsivity, and noise equivalent power (NEP) [4,6]. As a result, graphene photodetectors are not suitable for practical large-scale device applications. Recently, several attempts have been made to enhance the absorption of light and the performances of graphene-based photodetectors, for example, the photodetector coupling microcavities and plasmonics resonators to graphene [8–11], photodetector based on vertical p–n graphene

---

[*] *Corresponding authors at:* SKKU Advanced Institute of Nanotechnology (SAINT), Sungkyunkwan University, Suwon 440-746, Republic of Korea (J.H. Cho and E. Hwang), School of Electrical and Electronic Engineering, Yonsei University, Seoul 120-749, Republic of Korea (J.-H. Ahn).

E-mail addresses: ahnj@yonsei.ac.kr (J.-H. Ahn), euyheon@skku.edu (E. Hwang), jhcho94@skku.edu (J.H. Cho).

[1] Y. Lee & S.H. Yu equally contributed to this work.

http://dx.doi.org/10.1016/j.carbon.2015.02.071

junctions [12,13], and coupled to colloidal quantum dots (QDs) or nono wires (NWs) [14–19].

The combination of graphene, which features a remarkably broad absorption band, and dye molecules (e.g., rhodamine 6G (R6G)), which have a high absorption cross-section, provided a very large photocurrent, an ultrahigh quantum efficiency. The main mechanisms underlying the ultrahigh performance of the dye-sensitized graphene photodetector involve enhanced light absorption and the implementation of a photocurrent gain arising from the photoexcited charges. In this hybrid structure, the π-bond between the dye molecules and the graphene facilitated photoexcited charge transfer between the two materials [20–22]. Thus, the accumulation of photo-excited electrons in the dye layer introduced effective gating behavior that produced a high hole current in the graphene layer. The enhanced photocurrent arose from the chemical potential difference, which increased the number of mobile charge carriers present in the graphene, rather than from the production of photo-excited electrons. The photocurrent gain mechanism, in which multiple charge carriers were generated from each incident photon [23,24], relied on the ratio of the photoexcited electron relaxation time in the dye layer to the carrier transit time in the graphene layer. In our device, the recombination process in the dyes is hindered by the electron transfer from graphene layer and the recombination time in the dyes was on the order of milliseconds, much longer than the transit time (on the order of picoseconds based on hole mobiliy value of ~1000 cm^2/V s) of the carriers (holes) in the graphene. These parameters guaranteed a high gain. The dye-sensitized graphene photodetector exhibited a responsivity of 460 A/W, an effective quantum efficiency of $\sim 10^5$%, a specific detectivity of $\sim 10^{10}$ Jones, and a broad spectral bandwidth across the ultraviolet, visible, and near-infrared. Note that the effective quantum efficiency (EQE) was defined here as $\eta_{eff} = \eta G$, where η and G are the external quantum efficiency and the gain of the device, respectively. The availability of many different dye molecules through a variety of synthetic routes enables the simple hybrid photodetectors to be tuned for a variety of functionalities.

Recently, the organic dye-MoS_2 hybrid photodetector was reported [25], which showed an enhanced performance compared with the properties of the pristine MoS_2 photodetectors. The charge transfer mechanism plays an important role for the high performance in the hybrid dye/MoS_2 photodetector. Upon comparing the hybrid dye/MoS_2 photodetector with the hybrid dye/graphene photodetector, we find that the graphene-based device shows much enhanced performance (for example, the responsivity of graphene based photodetector is two orders of magnitude higher than MoS_2 based photodetector, i.e., 1.17 A/W in MoS_2 *vs.* 460 A/W in graphene). In addition, due to the presence of the band gap in MoS_2 the charge transfer of the photoexcited electrons from the dye molecules to the MoS_2 layer is very slow. Thus, the MoS_2 based photodetector shows very slow response (~a few seconds), which makes the MoS_2-based graphene be less practical. In graphene-based photodetector, the rise and fall times were found to be shorter than 100 ms. Based on the results of the current paper, we note that the hybrid of organic dye and graphene can be used as an effective photo-gating device (i.e., a new concept of field-effect-transistor with photo-gating), which is obviously not possible in MoS_2-based hybrid structure. It is also possible that the generalization of the hybrid structure by combining one of two-dimensional materials (e.g., MoS_2, WSe_2, etc.) with dye molecules for a variety of graphene-based optoelectronic devices.

2. Experimental detail

2.1. *Graphene synthesis and device fabrication*

Graphene films were produced by the thermal CVD method using folded Cu foils (Alpha aser) as catalytic substrates. First, the Cu foil was placed in a quartz tube and heated up to 1000 °C with flowing 10 sccm H_2 at 50 mTorr. After 4 h at 1000 °C, the mixture of 5 sccm CH_4 and 10 sccm H_2 gases was flowed for another 2 h at 450 mTorr. The sample was then cooled rapidly to room temperature with flowing 10 sccm H_2 at the pressure below 50 mTorr. This thermal CVD process based on folded copper catalytic material resulted in a graphene film with an uniform monolayer coverage of 99% with large grain size up to 100 μm. After the synthesis of graphene on Cu foils, polymethylmetacrylate (PMMA) were coated onto the graphene film grown Cu foil by spin coating. The backside graphene film was then removed by reactive ion etching (RIE) with O_2 plasma (70 mTorr, 100 W, 2 s). After etching the Cu layer with wet etchants (0.2 M aqueous solution of ammoniumpersulfate), the remaining graphene films on the polymer support were transferred onto a SiO_2/Si substrate containing the source and drain electrodes (Cr/Au, 3 nm/30 nm) formed by thermal evaporation. The channel width and length were 1000 and 50 μm, respectively. The PMMA support was then removed using acetone boiled up to 80 °C. The graphene patterns were formed by photolithography and reactive ion etching (RIE) with O_2 plasma. The R6G (Aldrich Co., 10^{-3} M in deionized water) and N719 (Aldrich Co., 30 mM in ethanol) organic dye molecules were drop-cast onto the device surface.

2.2. *Device measurement*

All current–voltage (I–V) and photodetecting properties of the graphene photodetectors were measured using Agilent 4155 semiconductor parameter analyzer under dark and illuminated conditions. The light sources were set up based on the monochromatic lasers (Susemicon) which have different wavelength from 400 to 980 nm at optical power of 4 mW (beam radius ~3 μm). The optical power was controlled from 1 μW to 2 mW using an optical attenuator (Thorlabs NDC-50C-4M) and was measured by laser power meter (Thorlabs PM 100D).

3. Results and discussion

3.1. *Spectral response of dye-sensitized graphene photodetector*

The dye-sensitized graphene photodetector was fabricated on a SiO_2/Si substrate. Highly n-doped Si wafers were employed as the gate electrode, and a thermally grown 300 nm thick SiO_2 layer was employed as a gate dielectric. The surface of the SiO_2 dielectric was then modified with n-octadecyltrimethoxysilane (ODTS) to reduce charge trapping by the silanol groups on SiO_2 [26]. Au source/drain electrodes were vacuum-deposited through a shadow mask onto the substrate to form channels 50 μm in length and 1000 μm in width. After transferring the CVD-grown monolayer graphene onto the substrate, photolithography and subsequent O_2 plasma etching were carried out to pattern the graphene channels [27]. The R6G organic dye molecules were deposited by drop-cast onto the graphene surface.

A schematic diagram and optical microscopy top view image of the dye-sensitized graphene photodetector are shown in Fig. 1a. Fig. 1b shows the calculated joint density of states (DOS) of the hybrid system prepared from graphene and R6G. The level alignment between the highest occupied molecular orbital (HOMO) and the lowest unoccupied molecular orbital (LUMO) of R6G with respect to the graphene energy band was determined through a series of density functional theory (DFT) calculations (see supporting materials for details) [28–30]. The calculated DOS of the hybrid system revealed that the Dirac point of graphene was located at the approximate center of the energy gap between the HOMO and LUMO of R6G. Fig. 1c shows the ultraviolet–infrared absorption spectra of R6G and the hybrid system composed of R6G and graphene. Both the pristine R6G and the hybrid system displayed an absorption peak at ~530 nm corresponding to the direct transition from the HOMO to the LUMO of R6G [31,32]. Unlike the pristine R6G, the hybrid system displayed an onset absorption at $\lambda_{\text{onset}} \sim 1050$ nm due to the transition of the photoexcited electrons in graphene to the LUMO of R6G. Since λ_{onset} was less than the energy band gap of R6G, the transition was not allowed in R6G. Importantly, the spectral absorption in the hybrid system was enhanced at all wavelengths $\lambda < \lambda_{\text{onset}}$ compared with the absorption of graphene.

Before implementation of photoresponse measurement about the hybrid photodetectors, we investigated photoresponse properties of the pristine graphene-based photodetector with the same device geometry as the R6G-graphene hybrid photodetector (see Fig. S2). In pristine graphene photodetector (i.e., without photogating effect) we found photocurrent in the order of nA as observed in other papers [5,6,10,17]. The photoresponse characteristics of the dye-sensitized photodetector were investigated. Figs. 2–4 show the performance of the photodetector made of graphene and R6G dye molecules. We have also studied the dye-sensitized graphene photodetector based on another dye molecule (i.e., Ru-based dye molecules, N719), and the results are shown in the supporting materials (see Figs. S3 and S4). Fig. 2a shows the total drain current (dark current plus photocurrent) as a function of the gate voltage at different illumination wavelengths over the range 400–980 nm. The photocurrent was measured at a fixed drain voltage of 0.1 V and a fixed incident illumination power of 1 mW. The black line indicates the dark current. The measured hole mobility of device was 870 $cm^2/V\,s$. Under all illumination wavelengths, the photocurrent (~mA) generated at a zero gate voltage in the hybrid photodetector was much higher than that (<μA) generated in a pristine graphene photodetector under the same illumination conditions. In addition to a high photocurrent intensity, the Dirac point was found to be shifted toward a positive gate voltage. Two distinct Dirac point shifts, divided by the characteristic wavelength ($\lambda_c = 530$ nm), were observed. These shifts corresponded to the energy gap between the HOMO and LUMO of R6G. The Dirac point shift at short wavelengths (i.e., $\lambda < \lambda_c$)

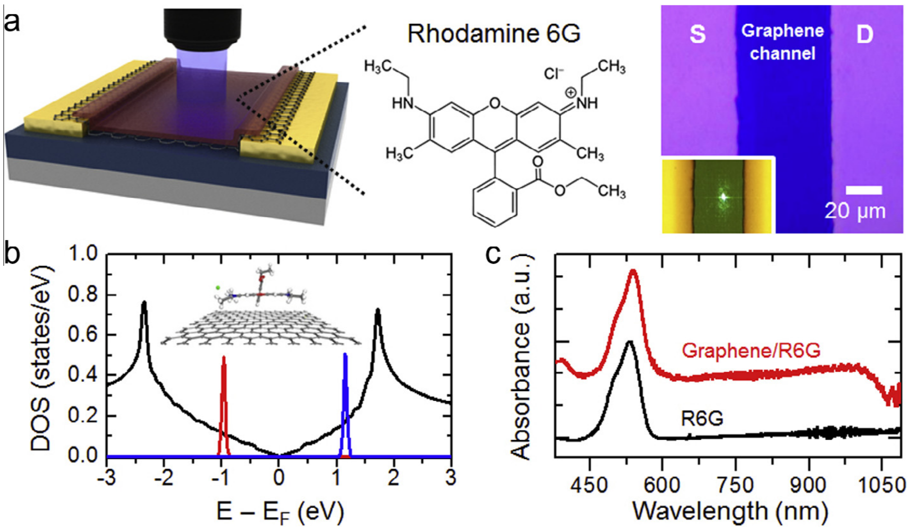

Fig. 1 – Dye-sensitized graphene photodetector. (a) Schematic diagram and optical microscopy top-view images of the dye-sensitized graphene photodetector device. (b) Calculated joint density of states (DOS) of the graphene-R6G hybrid structure. The black line represents the DOS of the graphene. The positions of the HOMO (blue) and LUMO (red) levels were obtained from B3PW91 calculations of the physisorbed R6G molecule. The HOMO of this structure was located at −0.971 eV and the LUMO was located at 1.150 eV with respect to the location of the Dirac point of graphene. (c) UV-IR absorption spectra of R6G and R6G/graphene hybrid films. The red line was arbitray shifted upward to distinguish the absorbance of R6G from that of R6G/graphene hybrid films. (A color version of this figure can be viewed online.)

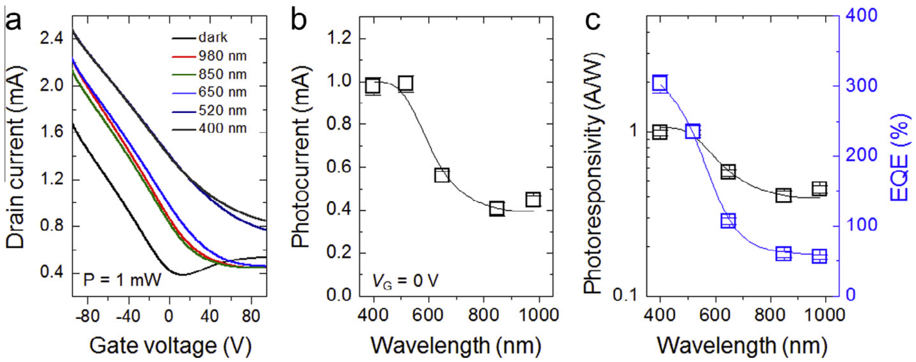

Fig. 2 – Wavelength-dependent photoresponse characteristics of the dye-sensitized graphene photodetector. (a) Transfer characteristics (V_D = 0.1 V) of the dye-sensitized graphene photodetector under different illumination wavelengths at a fixed incident illumination power of 1 mW. (b) Photocurrents at V_G = 0 V of the dye-sensitized graphene photodetector as a function of the illumination wavelength. (c) Responsivity (*R*) and effective quantum efficiency (EQE) *vs.* wavelength of the illumination source. (A color version of this figure can be viewed online.)

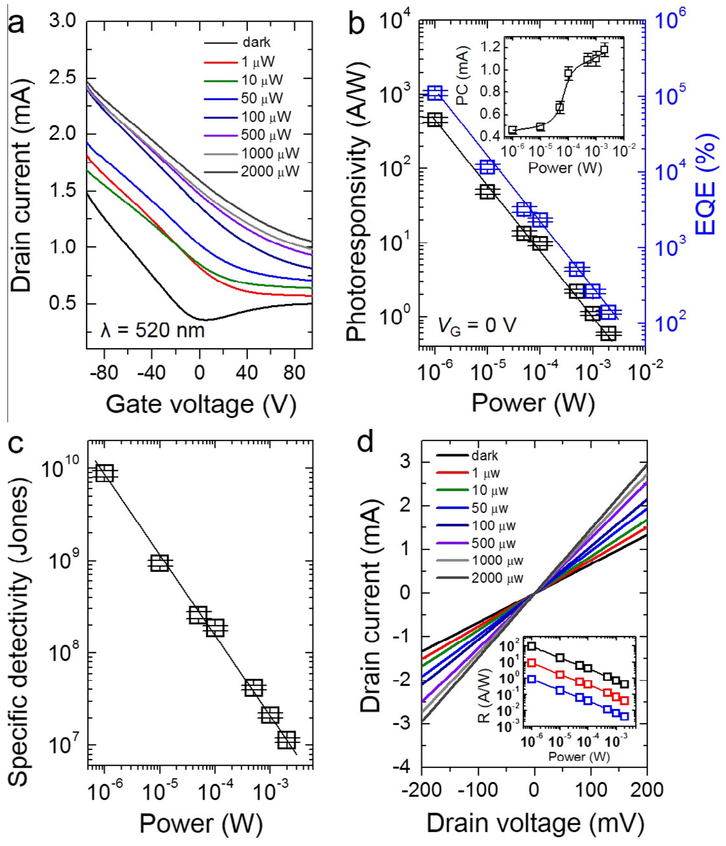

Fig. 3 – Illumination power-dependent photoresponse characteristics of the dye-sensitized graphene photodetector. (a) Transfer characteristics (V_D = 0.1 V) of the dye-sensitized graphene photodetector under different illumination powers at a fixed wavelength of 520 nm. (b) *R* and EQE as a function of the illumination power. The inset shows the photocurrent at V_G = 0 V as a function of the illumination power. (c) Specific detectivity (D^*) as a function of the illumination power. (d) Plot of the drain current *vs.* the drain voltage under various illumination powers. The inset shows *R* at three different drain voltages (black: 100 mV, red: 10 mV, blue: 1 mV) as a function of the illumination power. (A color version of this figure can be viewed online.)

was larger than the corresponding shift at long wavelengths (i.e., $\lambda > \lambda_c$). Consequently, the measured photocurrent for $\lambda < \lambda_c$ at a zero gate voltage was larger than the corresponding value at $\lambda > \lambda_c$. The change in the photocurrent (i.e., the difference between the total drain current and the dark current) is summarized in Fig. 2b and c shows the responsivity (black line) and the effective quantum efficiency (EQE) (blue line) as a function of the wavelength of incident light,

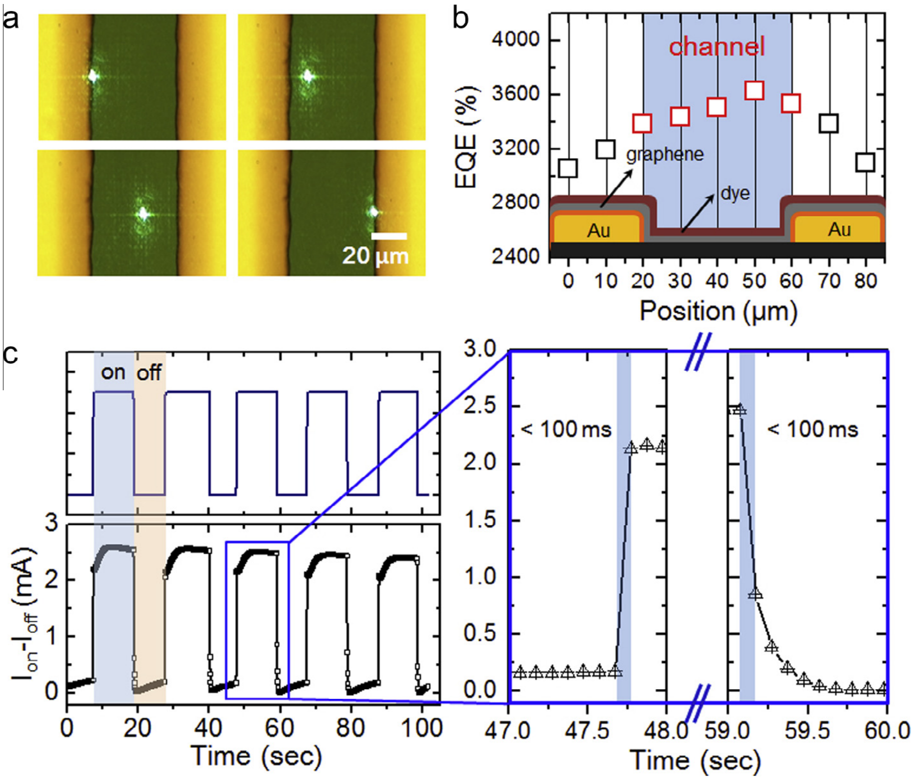

Fig. 4 – Spatial and photo-switching characteristics of the dye-sensitized graphene photodetector. (a) Optical microscopy images resulting from scanning an illumination laser spot across the graphene channel of the dye-sensitized graphene photodetector. (b) EQE values under laser illumination (100 μW, 520 nm) at different illumination positions. (c) Photo-switching characteristics of the device under alternating dark and light illumination (3 mW, 520 nm). The right panel shows an enlarged view of the temporal photocurrent response during on–off illumination switching. (A color version of this figure can be viewed online.)

measured at a zero gate voltage. The responsivity of a photodetector is defined as I_{ph}/P, where I_{ph} and P are the photocurrent and incident illumination power, respectively. The responsivity is related to the EQE, according to $(I_{ph}/e)/(P/h\upsilon)\times 100 = R \times E \times 100$, where R and E are the responsivity and the incident photon energy. As the wavelength decreased, both the responsivity and the EQE increased, with a large step at λ_c. Very high responsivity and EQE values were obtained, even at relatively high illumination powers (1 mW) at all wavelengths. Our device exhibited a responsivity of ~460 A/W and an EQE of ~10^5%, under an illumination power of 10^{-6} W (see Fig. 3b), which is the lowest power limit in our experimental setup. In general, the responsivity increases as the illumination power decreases until reaching saturation at very low power [26]. Based on our measurement (i.e., $R \propto P^{-1}$), the responsivity is expected to easily exceed 10^6 A/W at an illumination power of 1 pW if the relation between R and light power keeps down to that value. These behaviors (i.e., the Dirac point shift and the step in the photocurrent) could be understood in terms of the charge transfer between the graphene and R6G and the joint DOS of the hybrid system composed of graphene and R6G. As shown in Fig. 1b, the calculated DOS of the hybrid system revealed that the Dirac point of graphene was located approximately in the middle of the band gap between the HOMO and the LUMO of R6G. For incident photon energies less than the R6G energy gap (530 nm), photoexcited electrons in the graphene were transferred to R6G if the energies of the electrons exceeded the LUMO level of R6G. This process resulted in the accumulation of an excess of negative charges in R6G (Dirac voltage shift for $\lambda_c < \lambda < \lambda_{onset}$). Graphene could easily combine with R6G through π-bonds, which induced the transfer of photoexcited carriers in one layer to the other layer, and vice versa [20–22]. Photon energies exceeding the R6G gap induced light absorption and generated an electron–hole pair in the dye molecules due to a direct transition of the electrons from the HOMO to the LUMO. In this case, the electrons in graphene were transferred to the HOMO of the dye molecules, where they recombined with holes in the HOMO level to generate an excess of negative charges in R6G (Dirac voltage shift for $\lambda < \lambda_c$). Despite the different charge transfer behaviors, both cases induced the same type of excess charge (i.e., electrons) in the dye molecules, which acted as an effective negative gate voltage. Two distinct Dirac point shifts, separated by $\lambda_c = 530$ nm, could be understood in terms of the number of accumulated electrons in the dye molecules.

3.2. *Illumination power dependence of dye-sensitized graphene photodetector*

The illumination power-dependent photoresponse characteristics of the dye-sensitized photodetector were investigated. Fig. 3 shows the device performance at $\lambda = 520$ nm, which is shorter than the characteristic wavelength (λ_c). The results for longer wavelength (e.g., $\lambda = 980$ nm) than λ_c are shown in Fig. S5. Fig. 3a shows the total drain current as a function of the gate voltage under different illumination powers and at a fixed drain voltage of 0.1 V and a fixed illumination wavelength of 520 nm. The total device current increased gradually as the light power increased. This result supported the photogating mechanism proposed above: the number of photo-excited electrons from R6G increased with the illumination power and introduced a negative effective voltage in the graphene layer. As a result of this effective negative gating, the Dirac point shifted to larger positive gate voltages, and a greater hole current was introduced in the graphene layer at higher illumination powers. The illumination power-dependent spectral photocurrent at a zero gate voltage is summarized in the inset of Fig. 3b. We observed a very high photocurrent on the milliamps scale, even for a very low illumination power (0.45 mA at 10^{-6} W). Fig. 3b shows the responsivity (black line) and EQE (blue line) as a function of the illumination power. The dye-sensitized photodetector exhibited an EQE of 10^5% for an optical power on the microwatts scale. A higher EQE value was expected at even lower optical power levels. An important photodetector characteristic is the specific detectivity (D^*), which is measured in units of Jones. D^* is defined as $(A\Delta f)^{1/2}R/i_n$, where A is the effective area of the detector, Δf is the electrical bandwidth, R is the responsivity, and i_n is the noise current [15,33,34]. Fig. 3c shows D^* of the dye-sensitized graphene photodetector as a function of the light power. The measured D^* exceeded 10^{10} Jones at 1 μW. The specific detectivity is expected to exceed 10^{16} Jones at an illumination power of 1 pW, because the value increases as the illumination power decreases. Devices that operate at low voltages offer an efficient power consumption profile. It is important, therefore, to achieve a high photoresponse at a low drain voltage. Fig. 3d shows the total current as a function of the drain voltage for different illumination powers at =520 nm and at a zero gate voltage. The change in the current was proportional to both the applied drain voltage and the incident illumination power. The responsivity is plotted for different drain voltages in the inset of Fig. 3d. The responsivity was proportional to the applied drain voltage, but inversely proportional to the illumination power. A high responsivity of 1 A/W was observed, even at a very low drain voltage of 1 mV.

3.3. *Spatial and temporal response of dye-sensitized graphene photodetector*

The dye-sensitized photodetector was remarkably photosensitive across the entire device area. Fig. 4a shows the device response during spatial scanning of a laser spot across the channel area. The focused 520 nm laser beam was 3 μm in size and delivered an illumination power of 100 μW at the device surface. Fig. 4b, red (black) squares, indicate the EQE values measured inside (outside) of the graphene channel. In contrast to the photocurrents measured in graphene-based photodetectors, which generated a photocurrent across the metal contact area or in the center of the device, our hybrid photodetector generated a uniform EQE along the entire channel area, and none of the regions were characterized by significantly lower EQE values. In this hybrid structure, the photo-excited charges near the interface between R6G and graphene contribute mainly to the photogating effect. The drop-casted R6G film covers all graphene area and the average film thickness is far above the photogating saturation level. Thus, the uniform photocurrent response can be obtained across the photodetector area. A uniform response across the photodetector area is important in practical applications. Finally, we measured the time-resolved photoresponse of the hybrid photodetector under an illumination power of 3 mW, using the 520 nm laser beam. Fig. 4c shows the pulsed laser illumination (top) and the temporal response of the photocurrent (bottom). The rise and fall times were found to be shorter than 100 ms. The dye-sensitized graphene photodetector displayed a short temporal response that was attributed to the easy transfer of photoexcited electrons between the dye molecules and the graphene as a result of the weak π-bonds [20,21].

4. Summary

We developed a novel hybrid photodetector consisting of graphene and dye molecules. The dye-sensitized photodetector responded to the incident illumination over a broad wavelength range ($400 < \lambda < 1000$ nm). The responsivity and effective quantum efficiency were extremely high and exceeding 460 A/W and 10^5% at relatively high illumination power of 1 μW, respectively. The hybrid graphene photodetector displayed several advantages over other approaches: the device could be operated at low voltages and the photoresponse did not vary significantly across the detector area.

Although this report describes the ultra-high performance of a novel hybrid photodetector, the device may certainly be further optimized. Low-mobility CVD-grown graphene was used here, and graphene with a higher mobility (e.g., graphene on an h-BN substrate) may further increase the photocurrent gain [35,36]. The carrier transit time in higher-mobility graphene is much shorter than in low-mobility graphene. Consequently, the photocurrent gain in the higher-mobility graphene is expected to be higher. Organic dye molecules undergo photobleaching by photo-induced oxidation under light illumination, which may decrease the performance of the dye-sensitized graphene photodetector [32]. Therefore, encapsulation of the dye-sensitized graphene photodetectors is required to ensure good device photostabilities [37]. The graphene photodetector developed here was prepared with R6G and N719; however, many other dye molecules may be substituted to satisfy certain application-specific device specifications. Thousands of alternative dye molecules with comparable optical properties are available and may be readily adapted to the photodetector described here. The photodetectors, which offer a high responsivity, a uniform photoresponse, and good sensitivity to illumination in the infrared, visible, and ultraviolet regions, may be suitable for a variety of practical large-scale applications in flexible and transparent optoelectronics. Graphene optoelectronic devices may find utility in the development of cost-effective inter- and intra-chip optical communication technologies.

Acknowledgements

This work was supported by Basic Science Research Program (2013R1A1A2011897, 2009-0083540, and 2014R1A2A2A01006776) of the National Research Foundation of Korea (NRF) funded by the Ministry of Science, ICT & Future Planing, Korea. H. Kim acknowledges the provision of DGIST basic research program (14-NB-04) through MSIP. J. Jeon and H. Kim acknowledge the support by the Global Frontier R&D Program (2013-073298) on Center for Hybrid Interface Materials (HIM) funded by the Ministry of Science, ICT & Future Planning.

Appendix A. Supplementary data

Supplementary data associated with this article can be found, in the online version, at http://dx.doi.org/10.1016/j.carbon.2015.02.071.

REFERENCES

[1] Bonaccorso F, Sun Z, Hasan T, Ferrari A. Graphene photonics and optoelectronics. Nat Photonics 2010;4(9):611–22.
[2] Sarma SD, Adam S, Hwang E, Rossi E. Electronic transport in two-dimensional graphene. Rev Mod Phys 2011;83(2):407–70.
[3] Xia F, Mueller T, Lin Y-m, Valdes-Garcia A, Avouris P. Ultrafast graphene photodetector. Nat Nanotechnol 2009;4(12):839–43.
[4] Mueller T, Xia F, Avouris P. Graphene photodetectors for high-speed optical communications. Nat Photonics 2010;4(5):297–301.
[5] Park J, Ahn Y, Ruiz-Vargas C. Imaging of photocurrent generation and collection in single-layer graphene. Nano Lett 2009;9(5):1742–6.
[6] Xia F, Mueller T, Golizadeh-Mojarad R, Freitag M, Lin Y-m, Tsang J, et al. Photocurrent imaging and efficient photon detection in a graphene transistor. Nano Lett 2009;9(3):1039–44.
[7] Nair R, Blake P, Grigorenko A, Novoselov K, Booth T, Stauber T, et al. Fine structure constant defines visual transparency of graphene. Science 2008;320(5881):1308.
[8] Furchi M, Urich A, Pospischil A, Lilley G, Unterrainer K, Detz H, et al. Microcavity-integrated graphene photodetector. Nano Lett 2012;12(6):2773–7.
[9] Echtermeyer T, Britnell L, Jasnos P, Lombardo A, Gorbachev R, Grigorenko A, et al. Strong plasmonic enhancement of photovoltage in graphene. Nat Commun 2011;2(8):458–62.
[10] Liu Y, Cheng R, Liao L, Zhou H, Bai J, Liu G, et al. Plasmon resonance enhanced multicolour photodetection by graphene. Nat Commun 2011;2(12):579–85.
[11] Fang Z, Liu Z, Wang Y, Ajayan PM, Nordlander P, Halas NJ. Graphene-antenna sandwich photodetector. Nano Lett 2012;12(7):3808–13.
[12] Lemme MC, Koppens FH, Falk AL, Rudner MS, Park H, Levitov LS, et al. Gate-activated photoresponse in a graphene P–N junction. Nano Lett 2011;11(10):4134–7.
[13] Peters EC, Lee EJ, Burghard M, Kern K. Gate dependent photocurrents at a graphene Pn junction. Appl Phys Lett 2010;97(19):193102.
[14] Lin Y, Zhang K, Chen W, Liu Y, Geng Z, Zeng J, et al. Dramatically enhanced photoresponse of reduced graphene oxide with linker-free anchored Cdse nanoparticles. ACS Nano 2010;4(6):3033–8.
[15] Manga KK, Wang S, Jaiswal M, Bao Q, Loh KP. High-gain graphene-titanium oxide photoconductor made from inkjet printable ionic solution. Adv Mater 2010;22(46):5265–70.
[16] Konstantatos G, Badioli M, Gaudreau L, Osmond J, Bernechea M, de Arquer FPG, et al. Hybrid graphene-quantum dot phototransistors with ultrahigh gain. Nat Nanotechnol 2012;7(6):363–8.
[17] Zheng K, Meng F, Jiang L, Yan Q, Hng HH, Chen X. Visible photoresponse of single-layer graphene decorated with TiO_2 nanoparticles. Small 2013;9(12):2076–80.
[18] Guo W, Xu S, Wu Z, Wang N, Loy M, Du S. Oxygen-assisted charge transfer between Zno quantum dots and graphene. Small 2013;9(18):3031–6.
[19] Biroju RK, Giri PK, Dhara S, Imakita K, Fujii M. Graphene-assisted controlled growth of highly aligned Zno nanorods and nanoribbons: growth mechanism and photoluminescence properties. ACS Appl Mater Interfaces 2013;6(1):377–87.
[20] Xie L, Ling X, Fang Y, Zhang J, Liu Z. Graphene as a substrate to suppress fluorescence in resonance Raman spectroscopy. J Am Chem Soc 2009;131(29):9890–1.
[21] Ling X, Xie L, Fang Y, Xu H, Zhang H, Kong J, et al. Can graphene be used as a substrate for Raman enhancement? Nano Lett 2009;10(2):553–61.
[22] Zhou X, He S, Brown KA, Mendez-Arroyo J, Boey F, Mirkin CA. Locally altering the electronic properties of graphene by nanoscopically doping it with rhodamine 6G. Nano Lett 2013;13(4):1616–21.
[23] Munoz E, Monroy E, Garrido J, Izpura I, Sanchez F, Sánchez-Garcıa M, et al. Photoconductor gain mechanisms in Gan ultraviolet detectors. Appl Phys Lett 1997;71(7):870–2.
[24] Xie F, Lu H, Xiu X, Chen D, Han P, Zhang R, et al. Low dark current and internal gain mechanism of Gan Msm photodetectors fabricated on bulk Gan substrate. Solid-State Electron 2011;57(1):39–42.
[25] Yu SH, Lee Y, Jang SK, Kang J, Jeon J, Lee C, et al. Dye-sensitized Mos_2 photodetector with enhanced spectral photoresponse. ACS Nano 2014;8(8):8285–91.
[26] Wang X, Xu JB, Wang C, Du J, Xie W. High-performance graphene devices on Sio_2/Si substrate modified by highly ordered self-assembled monolayers. Adv Mater 2011;23(21):2464–8.
[27] Lee Y, Bae S, Jang H, Jang S, Zhu S-E, Sim SH, et al. Wafer-scale synthesis and transfer of graphene films. Nano Lett 2010;10(2):490–3.
[28] Perdew JP, Burke K, Ernzerhof M. Generalized gradient approximation made simple. Phys Rev Lett 1996;77(18):3865–8.
[29] Grimme S. Density functional theory with London dispersion corrections. Wiley Interdiscip Rev Comput Mol Sci 2011;1(2):211–28.
[30] Kim H, Choi J-M, Goddard III WA. Universal correction of density functional theory to include London dispersion (up to Lr, element 103). J Phys Chem Lett 2012;3(3):360–3.
[31] Kubin RF, Fletcher AN. Fluorescence quantum yields of some rhodamine dyes. J Lumin 1983;27(4):455–62.
[32] Avnir D, Levy D, Reisfeld R. The nature of the silica cage as reflected by spectral changes and enhanced photostability of trapped rhodamine 6G. J Phys Chem 1984;88(24):5956–9.
[33] Gong X, Tong M, Xia Y, Cai W, Moon JS, Cao Y, et al. High-detectivity polymer photodetectors with spectral response from 300 Nm to 1450 Nm. Science 2009;325(5948):1665–7.

[34] Liu S, Wei Z, Cao Y, Gan L, Wang Z, Xu W, et al. Ultrasensitive water-processed monolayer photodetectors. Chem Sci 2011;2(4):796–802.

[35] Dean C, Young A, Meric I, Lee C, Wang L, Sorgenfrei S, et al. Boron nitride substrates for high-quality graphene electronics. Nat Nanotechnol 2010;5(10):722–6.

[36] Konstantatos G, Levina L, Fischer A, Sargent EH. Engineering the temporal response of photoconductive photodetectors via selective introduction of surface trap states. Nano Lett 2008;8(5):1446–50.

[37] Zhao Y, Xie Y, Bao Z, Tsang YH, Xie L, Chai Y. Enhanced SERS stability of R6G molecules with monolayer graphene. J Phys Chem C 2014;118(22):11827–32.